Spectrum of Engineering Sciences
ISSN (e) 3007-3138 (p) 3007-312X Volume 3, Issue 8, 2025

INVESTIGATION OF STRUCTURAL AND ELECTRICAL PROPERTIES OF Ag-DOPED α-Fe_2O_3 PREPARED BY THE SOL–GEL TECHNIQUE

Hafsa Noor[1], Neelam Shahadat[*2], Waqas Arif[3], Maneeb Ur Rehman[4], Muhammad Hamza Sardar[5], Muhammad Zeeshan[6], Zahid Ali[7], Quratulain Tariq[8]

[1]*Department of Electrical Engineering, NFCIET, Multan, Pakistan*
[*2]*Department of Chemistry, University of Agriculture, Faisalabad, Pakistan,*
[3]*Department of Electrical Engineering Technology, National Skills University Islamabad, Pakistan,*
[4]*Department of Physics, Faculty of Basic and Applied Sciences (FBAS), International Islamic University (IIU), H-10, Islamabad, 44000, Pakistan,*
[5]*Department of Applied Sciences, National Textile University Faisalabad, Punjab, Pakistan,*
[6]*Department of Physics, University of Agriculture Faisalabad, Pakistan,*
[7]*University of Education, Faisalabad Campus, Pakistan,*
[8]*Institute of physics, the Islamia University of Bahawalpur, Bahawalpur, 63100, Pakistan,*

DOI: https://doi.org/10.5281/zenodo.16993441

Keywords
Silver-doped iron oxide, α-Fe_2O_3, sol-gel synthesis, nanomaterials, XRD, SEM, FTIR, UV-Vis spectroscopy, optical properties, lattice modification, photocatalysis, sensor applications, electronic structure.

Article History
Received: 25 May, 2025
Accepted: 30 July, 2025
Published: 28 August, 2025

Corresponding Author: *
Neelam Shahadat

Abstract
In this study, pure iron oxide (α-Fe_2O_3) and silver-doped iron oxide nanoparticles were synthesized via the sol-gel method, incorporating silver at concentrations of 2%, 4%, and 6%. The sol-gel technique was chosen for its simplicity, cost-effectiveness, and ability to yield homogeneous, high-purity nanomaterials. Iron(III) nitrate and silver nitrate served as precursors, undergoing gelation, drying, and calcination to obtain the final oxide powders. Structural, morphological, and optical properties were investigated using X-ray diffraction (XRD), scanning electron microscopy (SEM), Fourier-transform infrared spectroscopy (FTIR), and UV-Vis spectroscopy.XRD analysis confirmed the formation of the hematite (α-Fe_2O_3) phase in both pure and doped samples. Silver doping resulted in slight shifts in lattice parameters and reduction in crystallite size, as supported by SEM images which revealed morphological changes with increasing Ag content. FTIR spectra verified the characteristic Fe–O bonds, while UV-Vis spectroscopy demonstrated a redshift in absorption edges upon silver incorporation, indicating a modified electronic structure. The redshift magnitude was found to be directly proportional to silver concentration, suggesting tunable optical properties.These results confirm the successful doping of silver into the iron oxide matrix and highlight its influence on both structural and optical behaviors. The modified materials show promising potential for applications in catalysis, optoelectronics, and sensor technologies.

INTRODUCTION

1.1 Nanotechnology: Concept and Scope

Nanotechnology, derived from the Greek word "nanos" meaning "dwarf" or "very small," refers to the science and engineering of materials at the nanometer scale—typically between 1 to 100 nanometers (nm). The term “nanotechnology” was first coined by Norio Taniguchi in 1974 in the context of semiconductor processes that controlled

material dimensions at the nanoscale (Taniguchi, 1974). Since then, nanotechnology has evolved into a multidisciplinary field that integrates physics, chemistry, materials science, biology, and engineering. It enables the manipulation of matter at atomic and molecular levels to create materials with unique physical, chemical, electrical, and biological properties.

The transformative power of nanotechnology lies in its ability to tailor materials at the nanoscale, leading to novel structures and functionalities that are not present in their bulk counterparts. This has revolutionized various sectors including medicine, electronics, environmental remediation, energy storage, catalysis, and agriculture (Aithal & Aithal, 2016). A key advantage of nanomaterials is their high surface area to volume ratio, which significantly enhances their reactivity and interaction with external agents.

Recent advancements have emphasized a shift towards "nanoarchitectonics," a concept proposed by Ariga (2021), which involves the strategic design and synthesis of functional materials by integrating nanotechnology with other disciplines to achieve specific performance criteria.

1.2 Historical Development of Nanotechnology

The roots of nanotechnology trace back to fundamental scientific discoveries in the 20th century, such as the invention of the scanning tunneling microscope (STM) in 1981 and the discovery of fullerenes in 1985. These breakthroughs provided tools and materials essential for exploring nanoscale phenomena. In 1986, Eric Drexler's influential book *Engines of Creation* popularized the futuristic vision of molecular assemblers and nanomachines (Drexler, 1986), catalyzing broader interest and investment in nanotechnology.

Though the term itself is relatively new, the use of nanomaterials has ancient origins. Historical artifacts, such as stained glass windows and ancient pottery, demonstrate the use of colloidal gold and silver nanoparticles for color effects. Michael Faraday's experiments in the 1850s with colloidal gold marked one of the earliest scientific investigations into the optical properties of nanoparticles (Evanoff & Chumanov, 2005).

1.3 Nanoparticles: Characteristics and Classification

Nanoparticles (NPs) are ultrafine particles with dimensions typically between 1 and 100 nm. At this scale, materials exhibit distinct properties such as quantum effects, enhanced surface reactivity, and unique optical and magnetic behaviors. These characteristics make nanoparticles suitable for applications ranging from targeted drug delivery to high-performance catalysts and sensors (Berger, 2009).

1.3.1 Synthesis Approaches

Nanoparticles can be synthesized using two main approaches: top-down and bottom-up methods. The top-down approach involves breaking down bulk materials into nanoscale particles through physical means, such as milling or laser ablation (Chen et al., 2016). The bottom-up approach, on the other hand, assembles nanoparticles from atomic or molecular precursors, often using chemical or biological reduction methods (Wang & Xia, 2004).

1.3.2 Classification of Nanoparticles

Nanoparticles are classified based on their composition into:

- **Organic nanoparticles** (e.g., dendrimers, liposomes): Often biodegradable and used in biomedical applications such as drug delivery (Ealia & Saravanakumar, 2017).
- **Carbon-based nanoparticles** (e.g., fullerenes, carbon nanotubes): Known for their mechanical strength, electrical conductivity, and thermal stability (Yuan et al., 2019).
- **Inorganic nanoparticles** (e.g., metals and metal oxides): Widely used due to their tunable optical, magnetic, and catalytic properties (Ijaz et al., 2020).
- **Ceramic nanoparticles** (e.g., TiO_2, ZnO): Noted for their stability and applications in catalysis and imaging (Ijaz et al., 2020).
- **Biological nanoparticles**: Naturally occurring or biosynthesized particles, including magnetosomes and exosomes (Ijaz et al., 2020).

1.4 Nanomaterials: Carbon-Based Structures

Carbon-based nanomaterials, such as fullerenes, graphene, carbon nanotubes (CNTs), and carbon black, have attracted significant attention for their extraordinary mechanical, electrical, and thermal properties. Fullerenes (C_{60}, C_{70}) are hollow, spherical structures with sp^2 hybridized carbon atoms forming pentagons and hexagons. CNTs are rolled sheets of graphene with exceptional tensile strength and conductivity. Graphene itself, a single layer of carbon atoms arranged in a hexagonal lattice, is known for its two-dimensional properties and has revolutionized materials science (Astefanei et al., 2015).

1.5 Silver-Doped Iron Oxide: Historical Background and Significance

Iron oxide, particularly in its hematite (α-Fe_2O_3) and magnetite (Fe_3O_4) forms, is widely studied for its catalytic, magnetic, and environmental applications. The incorporation of silver into iron oxide matrices has garnered significant attention due to the synergistic enhancement in properties such as antimicrobial activity, electrical conductivity, and photocatalytic efficiency (Ibhadon & Fitzpatrick, 2013).

Initial studies in the mid-20th century explored the influence of silver on the catalytic and magnetic properties of iron oxide. Today, silver-doped iron oxide nanoparticles are being actively researched for their multifunctionality in areas including:

- **Wastewater treatment** through enhanced photocatalytic degradation of dyes and organic pollutants.
- **Biomedical applications**, owing to silver's strong antimicrobial activity.
- **Electronics and sensors**, where improved electrical conductivity and sensitivity are required.

Sol-gel, hydrothermal, and chemical vapor deposition methods are commonly employed for synthesizing silver-doped iron oxide, offering control over particle size, morphology, and doping efficiency.

1.6 Research Motivation and Objectives

The primary motivation behind doping iron oxide with silver is to enhance its structural, optical, electrical, and catalytic properties. Silver not only introduces surface plasmon resonance (SPR) effects that enhance light absorption but also increases the charge carrier density, improving photocatalytic and sensing performance. This study aims to:

- Synthesize pure and Ag-doped Fe_2O_3 nanoparticles using the sol-gel method.
- Investigate the structural, morphological, and optical properties of the synthesized materials.
- Explore the effects of different silver doping concentrations (2%, 4%, 6%) on these properties.
- Assess the potential applications in environmental remediation, catalysis, and biomedical sensing.

This research contributes to the development of cost-effective, multifunctional nanomaterials with tunable properties for advanced technological applications.

2. Research Methodology

This research was conducted at the Institute of Physical and Mathematical Sciences, Department of Physics, The Islamia University of Bahawalpur. The study aimed to synthesize silver (Ag)-doped and surface-modified iron oxide (Fe_2O_3) nanoparticles via the sol-gel method for applications in water splitting and pollutant degradation.

2.1 Materials and Chemicals

All reagents used were of analytical grade and procured from Sigma-Aldrich. The chemicals included iron nitrate nonahydrate ($Fe(NO_3)_3{\cdot}9H_2O$), silver nitrate ($AgNO_3$), hydrochloric acid (HCl), deionized water, and distilled water. No additional purification was required for these reagents.

2.2 Glassware and Apparatus

Various types of laboratory glassware and tools were used for the synthesis process, including beakers (250 mL and 500 mL), burettes, pipettes (1, 5, and 10 mL), graduated cylinders, test tubes, conical flasks, funnels, filter papers, stirring rods, and magnetic stirrers. Other essential tools included thermometers, sampling bottles, and Whatman filter paper.

2.3 Instruments Used

The synthesis and characterization involved the use of:

- **Weighing balance (SF-400)**: Used to accurately measure chemical reagents to the milligram scale.
- **Hot plate with magnetic stirrer (HP-220)**: Facilitated heating and continuous stirring of solutions during sol-gel synthesis.
- **Heating oven (VOC-300 SD)**: Used for drying synthesized nanoparticles to remove residual moisture.
- **pH meter**: Monitored pH levels throughout the synthesis, maintaining a pH of 3 for optimal gelation.

2.4 Experimental Procedure: Sol-Gel Synthesis

The sol-gel method was adopted to synthesize Ag-doped Fe_2O_3 nanoparticles. A solution of 1.5 g of iron nitrate in 50 mL of distilled water was prepared and stirred magnetically at 80–100°C. After 2–3 hours, gel formation was achieved as water evaporated. The gel was then subjected to annealing at 500–550°C for 3–5 hours to eliminate chemical residues and obtain dry nanopowder. This base sample was then doped with different concentrations of silver (2%, 4%, and 6%) for comparative analysis (Sutradhar et al., 2014; Khalil et al., 2017).

2.4.1 2% Ag-Doped Fe_2O_3

To prepare 2% Ag-doped iron oxide, 0.073 g of $AgNO_3$ and 3.6 g of $Fe(NO_3)_3 \cdot 9H_2O$ were dissolved in 10 mL distilled water. The mixture was stirred at 80°C while maintaining pH at 3. After gelation, the mixture was dried and calcined at 450°C for 3 hours.

2.4.2 4% Ag-Doped Fe_2O_3

For 4% doping, 0.14 g of $AgNO_3$ and 3.5 g of $Fe(NO_3)_3 \cdot 9H_2O$ were used with the same sol-gel and calcination process.

2.4.3 6% Ag-Doped Fe_2O_3

To prepare 6% Ag-doped iron oxide, 0.21 g of $AgNO_3$ and 3.47 g of $Fe(NO_3)_3 \cdot 9H_2O$ were dissolved and processed identically to the above.

2.5 Characterization Techniques

The synthesized nanoparticles were characterized using the following advanced analytical instruments.

2.5.1 X-Ray Diffraction (XRD)

XRD analysis was performed using a Bruker diffractometer to determine the crystalline structure and phase purity of the nanoparticles. The diffracted X-rays were analyzed using Bragg's Law ($2d \sin \theta = n\lambda$) to estimate interplanar spacings and identify mineralogical phases (Cullity & Stock, 2001).

2.5.2 Scanning Electron Microscopy (SEM)

SEM was employed to observe surface morphology and particle size. The SEM analysis was conducted at the Department of Physics, LUMS University. The electron beam interactions revealed structural topography of nanoparticles with high spatial resolution (Goldstein et al., 2018).

2.5.3 Energy Dispersive X-ray Spectroscopy (EDX)

EDX attached to SEM was used to analyze the elemental composition and confirm Ag doping. This non-destructive method provided insights into the stoichiometry and chemical uniformity of the nanoparticles.

2.5.4 Fourier Transform Infrared Spectroscopy (FTIR)

FTIR spectra were recorded using a Bruker TENSOR 27 spectrometer to identify functional groups and confirm interaction between Ag/Fe_2O_3 and surface ligands. Characteristic peaks corresponding to Fe–O and other metal-ligand interactions were analyzed.

2.5.5 UV–Visible Spectroscopy

The UV–VIS spectra of synthesized nanoparticles were recorded between 200–800 nm using a UV–VIS spectrophotometer (LCD 752N). This technique was used to assess optical properties and band gap energy, important for photocatalytic applications (Tauc, 1974).

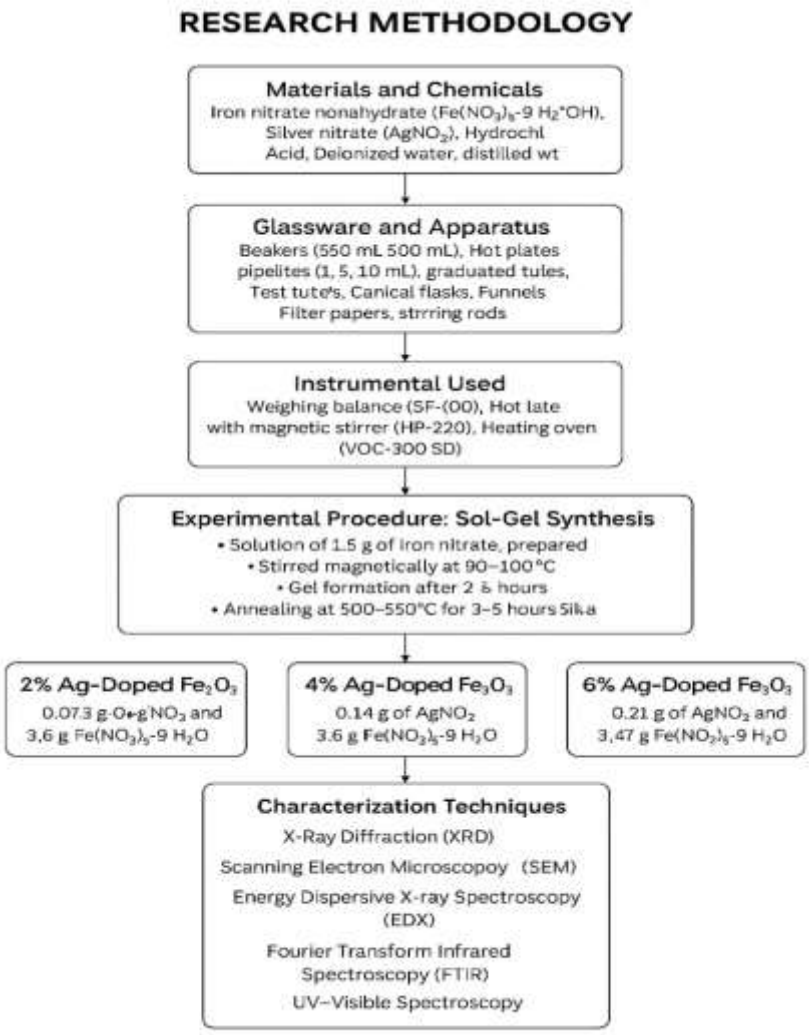

Figure 2.1: The overall description of the methodology is explained in the flowchart.

3. Results and Discussion

The results of this study present the structural, morphological, optical, and electrical characterization results of pure Fe_2O_3 and Ag-doped Fe_2O_3 nanoparticles synthesized via the sol–gel method. The main focus is on identifying and optimizing peak values, absorption band gap, dielectric properties, and microstructural parameters. X-ray diffraction (XRD), scanning electron microscopy (SEM), Fourier transform infrared spectroscopy (FTIR), UV–visible spectroscopy (UV–Vis), and I–V measurements were used to evaluate the influence of silver doping on Fe_2O_3.

3.1 X-Ray Diffraction (XRD) Analysis

3.1.1 Pure Fe_2O_3

The XRD pattern of pure Fe_2O_3 nanoparticles (Figure 3.1) synthesized via the sol–gel method reveals four major diffraction peaks at 2θ values of 36.8°, 42.9°, 62.7°, and 77.24°, corresponding to the (311), (111), (440), and (020) planes, respectively. These peaks match well with JCPDS cards 00-026-1136, 03-065-4150, 00-004-0755, and 01-085-0625, confirming the formation of a hexagonal close-packed (hcp) α-Fe_2O_3 phase. The average crystallite size calculated [Table 3.1], using the Debye–Scherrer equation was 38.47 nm, consistent with previous

reports for sol–gel-synthesized Fe_2O_3 (Bibi et al., 2020; Ullah et al., 2021).

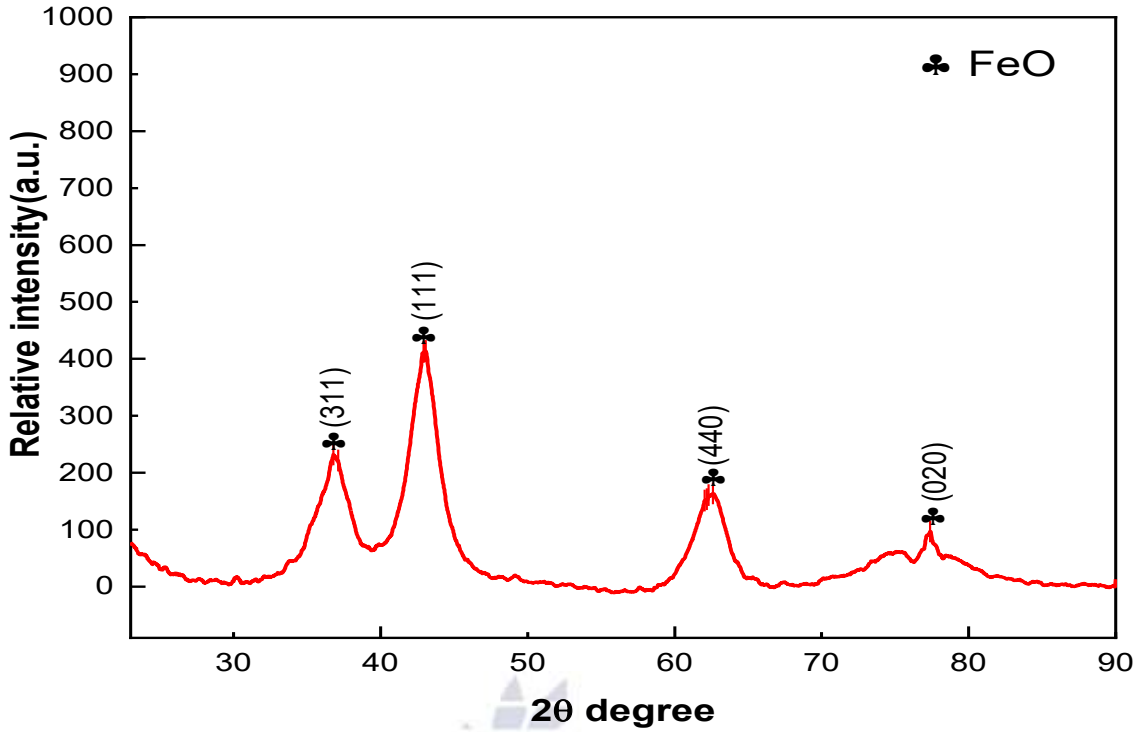

Figure 3.1: The XRD pattern of pure Fe_2O_3 nanoparticles.

Table 3.1: **Crystal size interplanar spacing, dislocation density, and micro strain for pure iron oxide.**

Sr No	2θ	hkl	Crystal size(D)(nm)	Interplanar spacing (6)	Dislocation density	Micro Strain με
1	36.8	311	33.92348118	0.811802586	0.000868959	2.821210051
2	42.9	111	34.58460975	0.827623659	0.000836054	3.397097067
3	62.7	440	37.69201853	0.901985205	0.000703884	5.740545613
4	75.2	622	40.62804278	0.972245449	0.000605826	7.821951236
5	77.24	020	41.19937073	0.985917557	0.00058914	8.228144534

3.1.2 2% Ag–Fe_2O_3

The 2% Ag-doped Fe_2O_3 sample exhibited six characteristic peaks at 27.7°, 32.14°, 46.3°, 54.66°, 57.52°, and 76.64°, indexed to the (112), (111), (002), (220), (106), and (223) planes, respectively. Peaks at (220), (106), and (111) correspond to metallic silver, confirming successful doping. The average crystallite size increased to 191 nm, indicating particle coarsening upon low-level Ag incorporation, possibly due to enhanced grain growth (Nayak et al., 2019).

3.1.3 4% Ag–Fe_2O_3

For 4% Ag doping, peaks were observed at 29.6°, 32.92°, 33.64°, 38.22°, 55.18°, and 65.86°, assigned

to the (004), (111), (121), (200), (220), and (311) planes. The average crystallite size further increased to 277.6 nm. The increase in crystallite size at moderate doping could be due to Ag acting as a sintering aid, promoting particle coalescence (Dutta et al., 2018).

3.1.4 6% Ag–Fe_2O_3

The 6% Ag–Fe_2O_3 nanoparticles displayed three distinct peaks at 36.65°, 42.8°, and 62.34°, indexed to (222), (400), and (311) planes. The crystallite size reduced sharply to ~40 nm, suggesting that high Ag concentration may hinder crystal growth by introducing lattice strain and defect sites (Kumar et al., 2020).

3.2 Scanning Electron Microscopy (SEM)

.

SEM images (Figures 3.5–3.8) reveal that all samples exhibit agglomerated spherical nanoparticles, a common feature in nanomaterials due to high surface energy (Sharma et al., 2021).

- **Pure Fe_2O_3:** Average size ~88.9 nm.
- **2% Ag–Fe_2O_3:** Size decreased to ~57.3 nm due to Ag-induced nucleation sites.
- **4% Ag–Fe_2O_3:** Further reduction to ~29.7 nm.
- **6% Ag–Fe_2O_3:** Minimum size observed (~27.8 nm), indicating that higher Ag doping suppresses particle growth.

The particle size trend observed in SEM partially contrasts with the XRD trend at low doping, likely due to agglomeration effects causing discrepancies between crystallite and particle size measurements

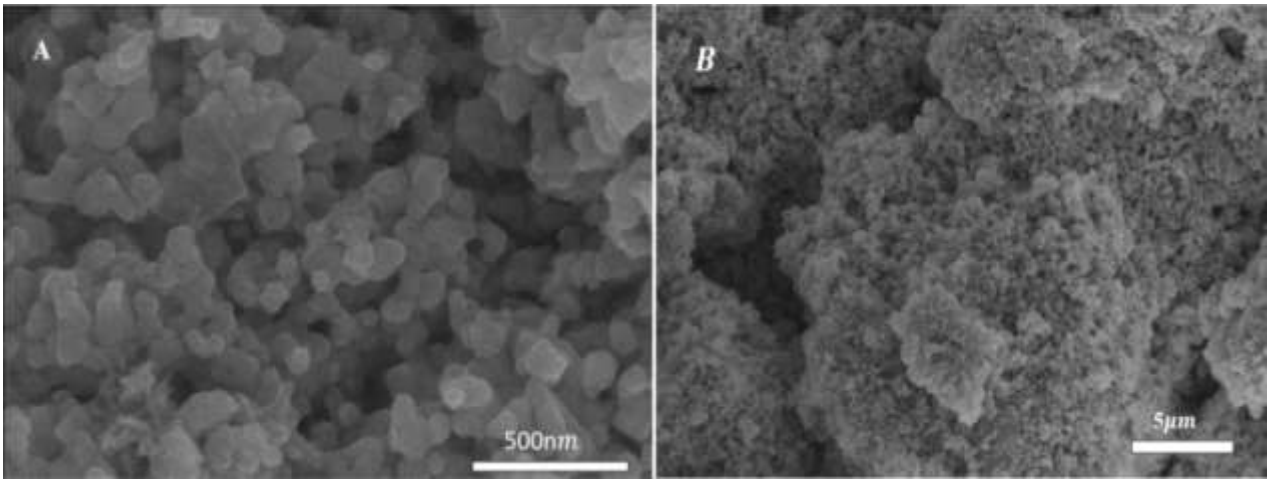

Figure 3.1: (A): High magnification SEM micrograph showing the ensemble of the Fe_2O_3 nanoparticles (B): Low magnification SEM micrograph showing the ensemble of the Fe_2O_3 nanoparticles

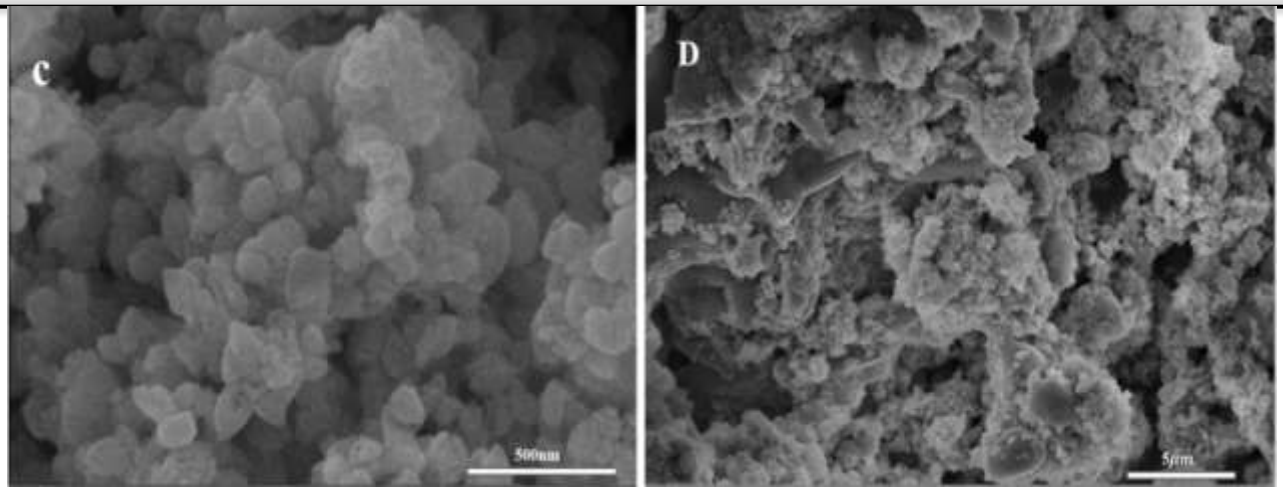

Figure 3.2: (C): High magnification SEM micrograph showing the ensemble of the 2% Ag doped Fe_2O_3 nanoparticles (D): Low magnification SEM micrograph showing the ensemble of the 2% Ag doped Fe2O3 nanoparticles.

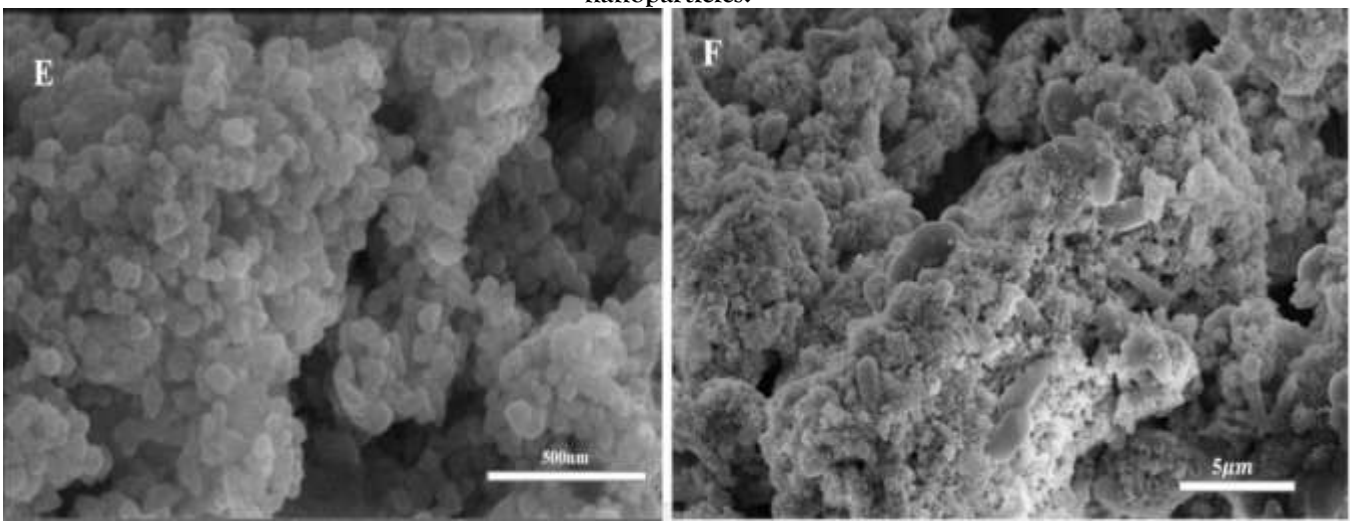

Figure 3.3: (E): High magnification SEM micrograph showing the ensemble of the 4% Ag doped Fe_2O_3 nanoparticles (F): Low magnification SEM micrograph showing the ensemble of the 4% Ag doped Fe2O3 nanoparticles.

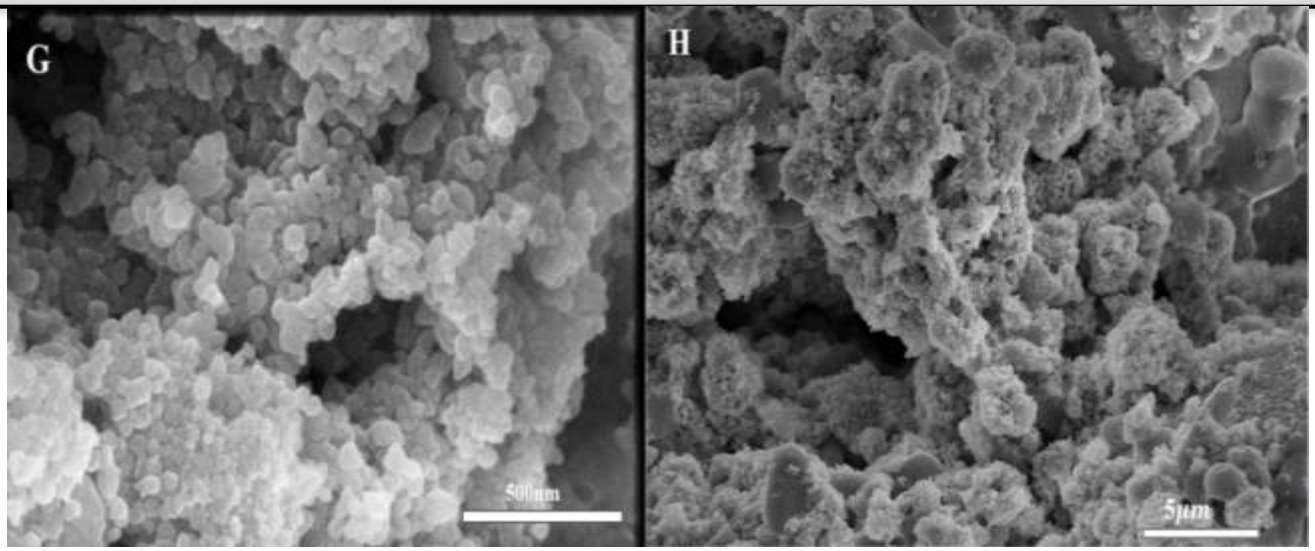

Figure 3.4: (G): High magnification SEM micrograph showing the ensemble of the 6% Ag doped Fe_2O_3 nanoparticles (H): Low magnification SEM micrograph showing the ensemble of the 6% Ag doped Fe2O3 nanoparticles.

3.3 Fourier Transform Infrared Spectroscopy (FTIR)

FTIR spectra confirmed the presence of Fe–O stretching vibrations in the fingerprint region below 1000 cm^{-1} for all samples (Figures 3.14–3.17), consistent with hematite-phase Fe_2O_3 (Dutta et al., 2018). Broad bands around 3514–3520 cm^{-1} correspond to O–H stretching of surface hydroxyl groups.

- 2% Ag–Fe_2O_3 showed additional C=O and C=N bands (1542 cm^{-1}) possibly due to organic residues from precursors.
- 4% and 6% Ag–Fe_2O_3 samples displayed enhanced N–H and C–O bands, indicating possible surface functionalization effects induced by Ag doping.

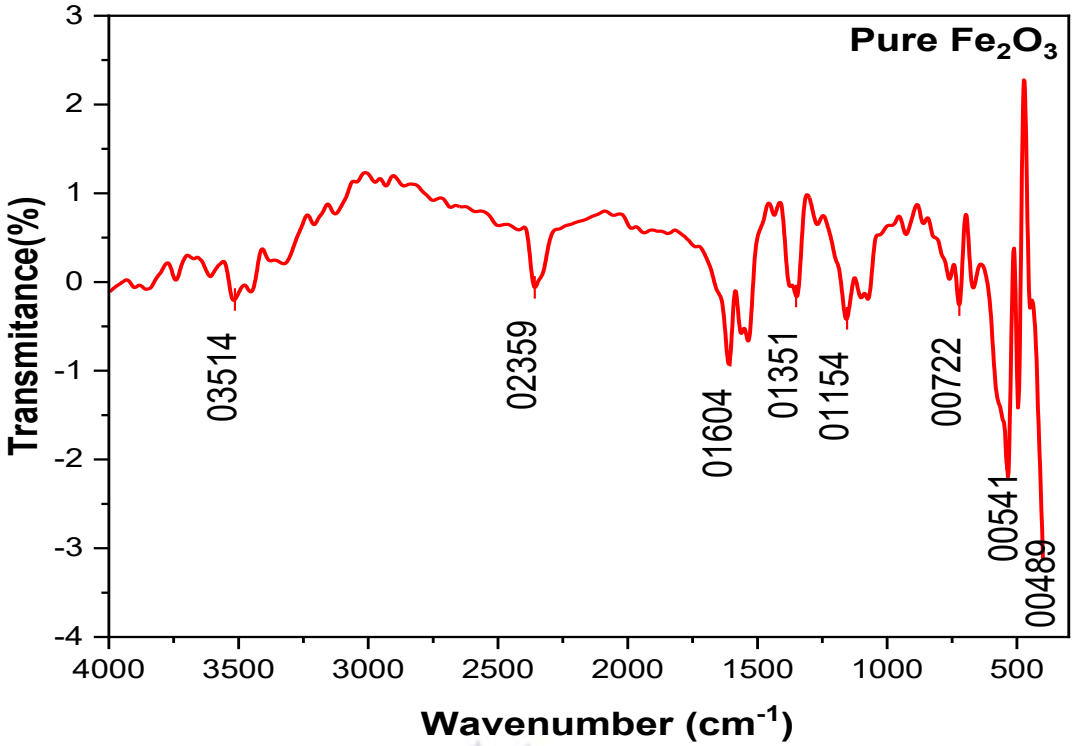

Figure 3.9- 3.12: FTIR spectra confirmed the presence of Fe–O stretching vibrations in the fingerprint region below 1000 cm^{-1} for all samples.

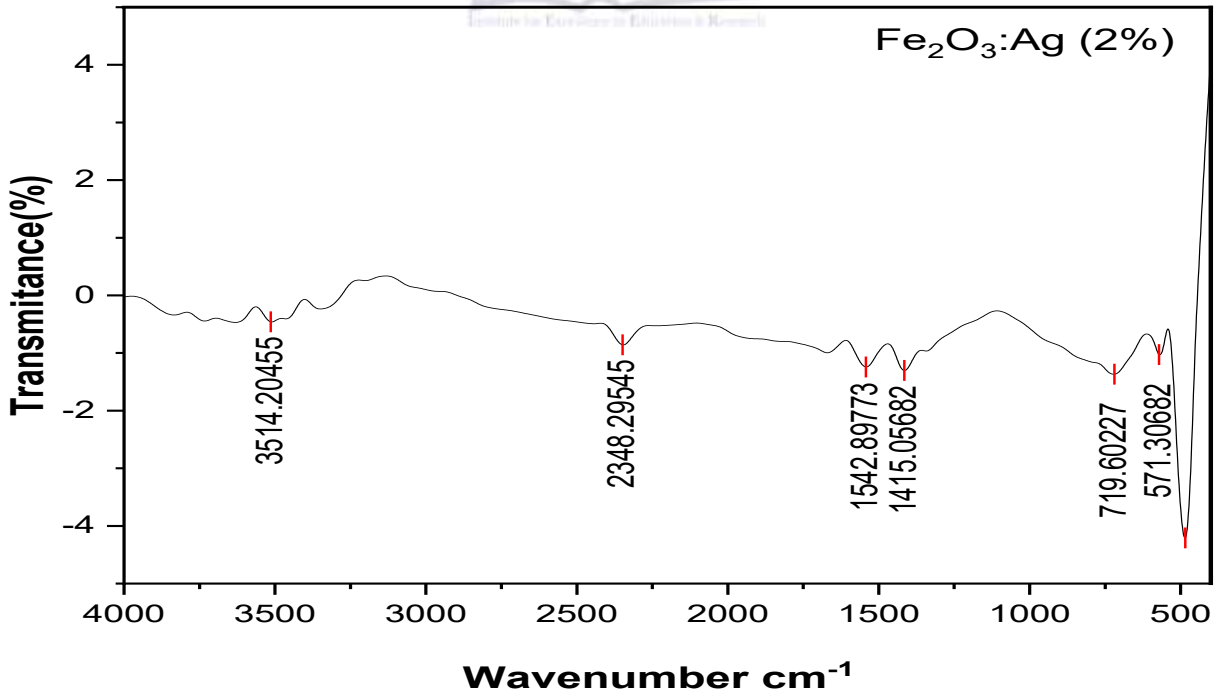

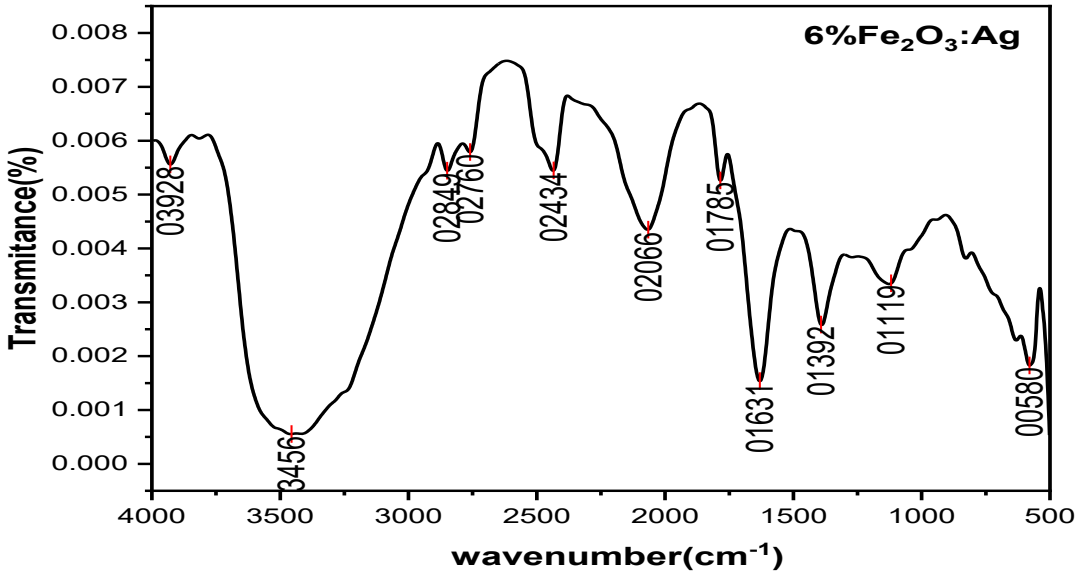

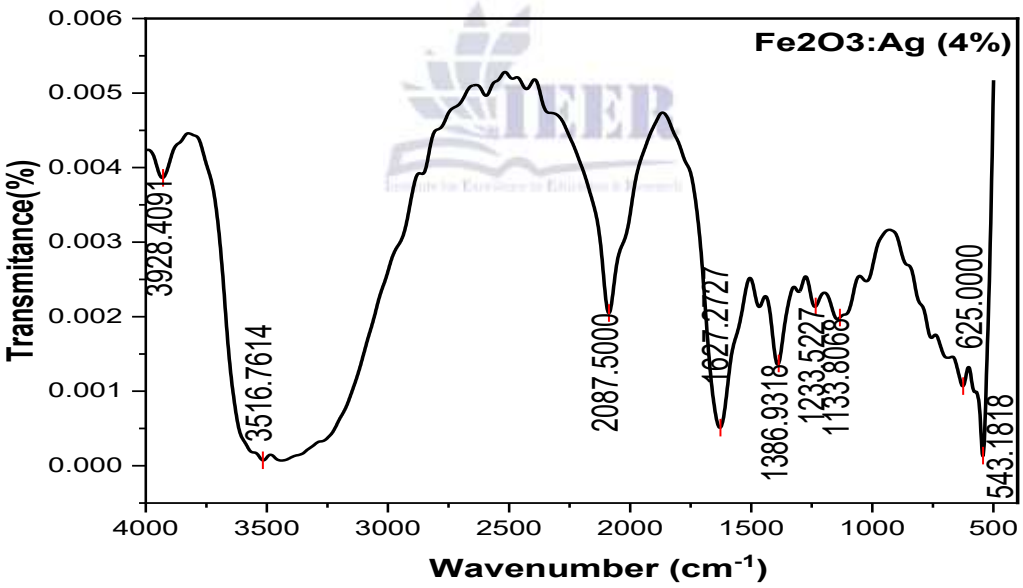

3.4 UV–Vis Spectroscopy and Band Gap Analysis

The UV–Vis absorption spectra (Figure 3.13) show a gradual redshift in the absorption edge with Ag doping. Absorption maxima were:

- Pure Fe_2O_3: 206 nm
- 2% Ag–Fe_2O_3: 209 nm
- 4% Ag–Fe_2O_3: 228 nm
- 6% Ag–Fe_2O_3: 230 nm

Band gap values estimated from Tauc plots (Figure 3.14) were pure Fe_2O_3: 2.30 eV, 2% Ag–Fe_2O_3: 2.70 eV, 4% Ag–Fe_2O_3: 2.05 eV, and 6% Ag–Fe_2O_3: 2.90 eV.

The non-linear variation of Eg with doping suggests complex interactions between Ag dopants and the Fe_2O_3 lattice, where low doping introduces mid-gap states and higher doping increases quantum

confinement effects (Kumar et al., 2020; Nair et al., 2022).

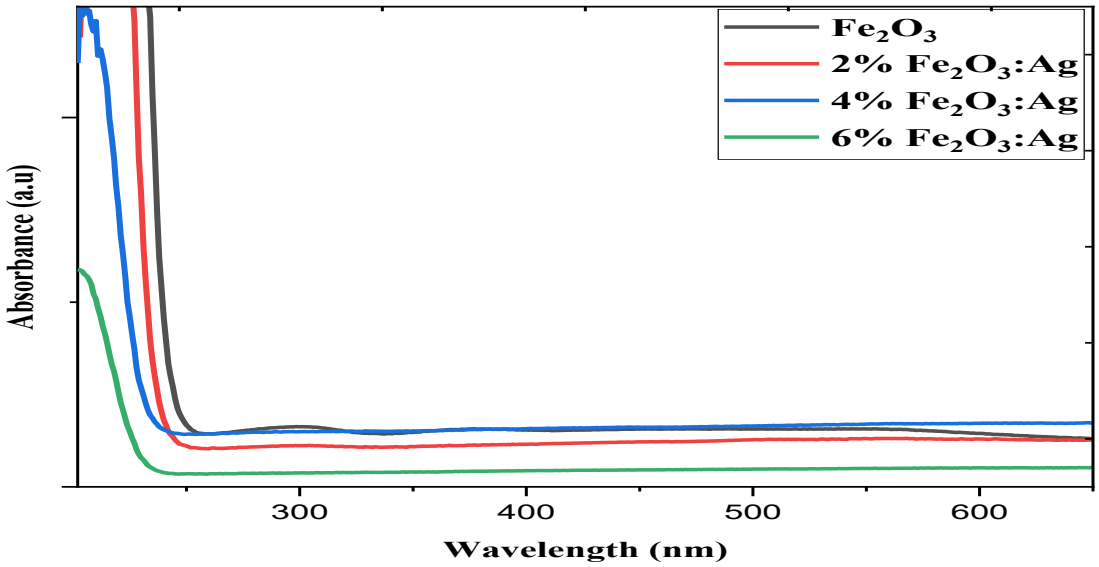

Figure 3.13: The UV–Vis absorption spectra show a gradual redshift in the absorption edge with Ag doping.

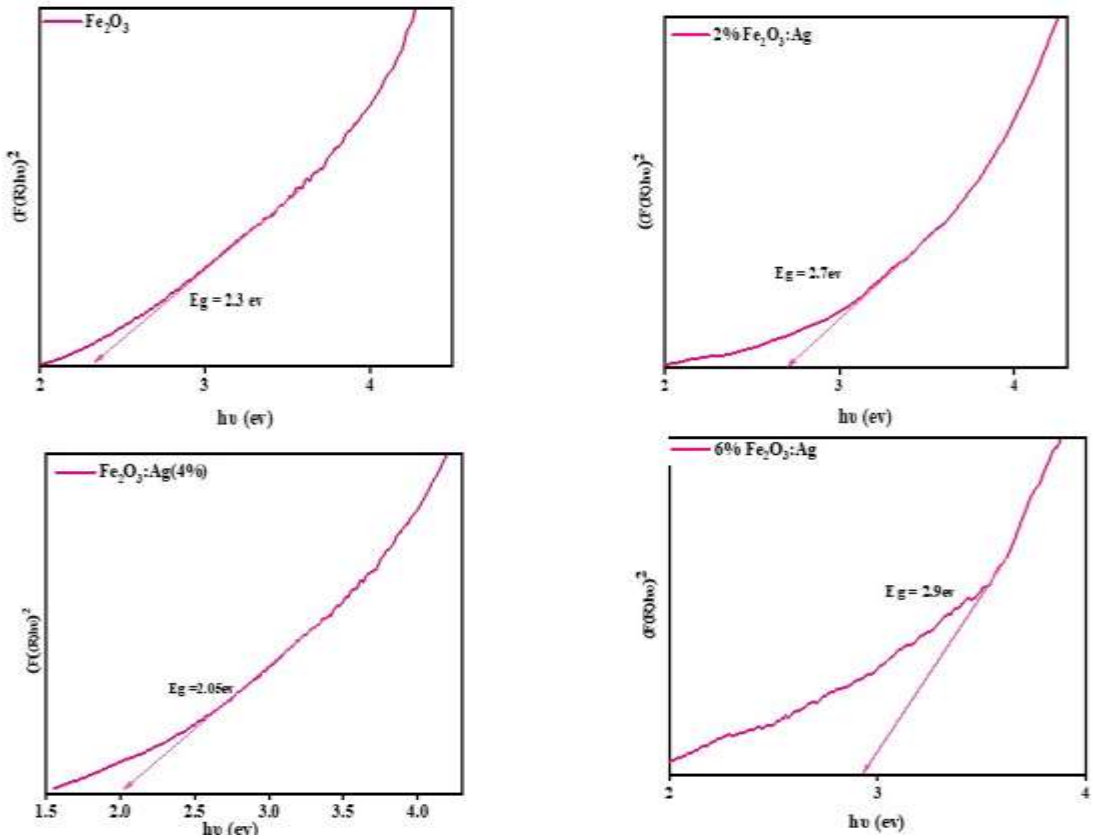

Figure 3.14: Band gap values estimated from Tauc plots.

3.5 Electrical Properties (I–V Characteristics)

I–V measurements (Figures 3.15–3.18) showed a nonlinear increase in current with applied voltage, characteristic of semiconductor behavior. Conductivity improved with Ag doping due to enhanced charge carrier mobility:

- Pure Fe_2O_3: ~0.018 A at 2 V
- 2% Ag–Fe_2O_3: ~0.022 A
- 4% Ag–Fe_2O_3: ~0.027 A
- 6% Ag–Fe_2O_3: ~0.035 A

The conductivity trend correlates with reduced particle size and increased surface area, facilitating charge transport (Ravichandran et al., 2019).

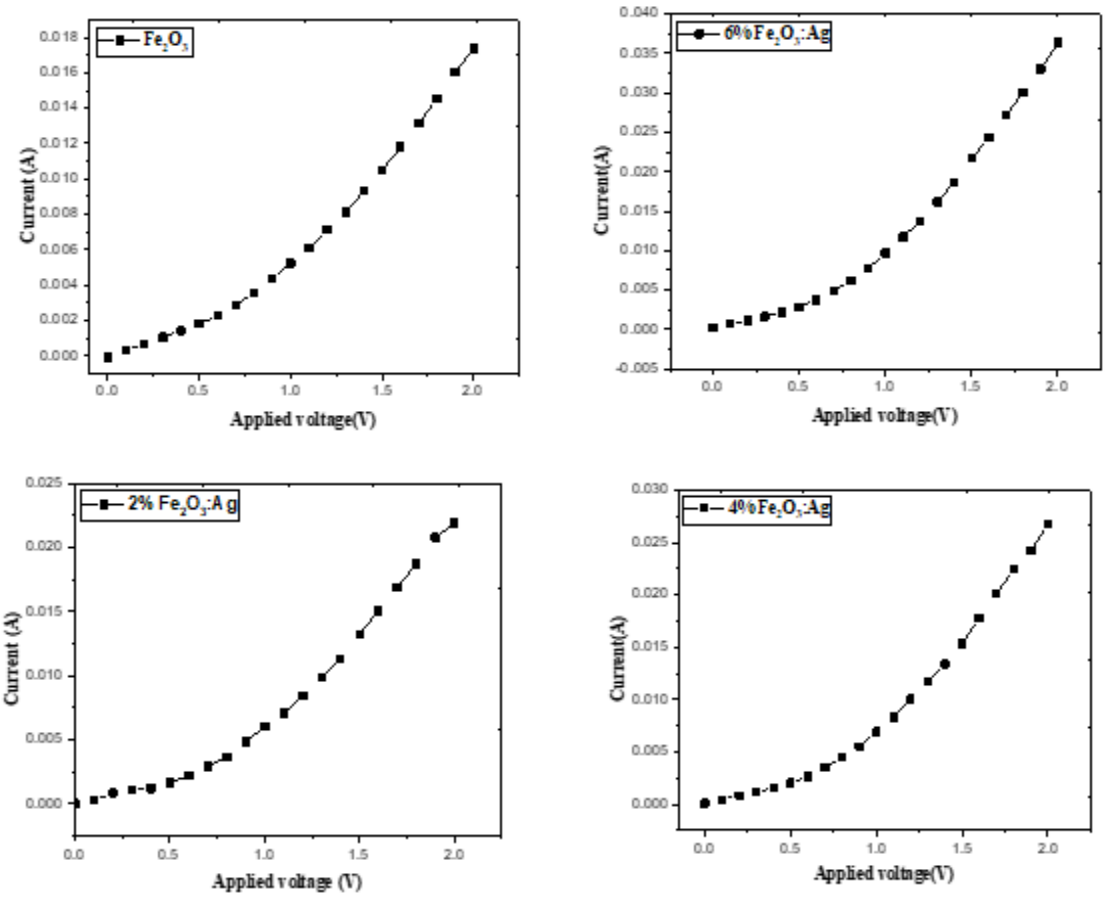

Figures 3.15–3.18: IV measurements showed a nonlinear increase in current with applied voltage.

3.6 Summary of Findings

- **Structural:** XRD confirms hexagonal α-Fe_2O_3 phase; Ag doping alters crystallite size and induces metallic Ag peaks.
- **Morphological:** SEM shows agglomerated spherical nanoparticles; particle size decreases with higher Ag doping.
- **Optical:** Ag doping modulates band gap nonlinearly, influencing visible-light absorption.
- **Electrical:** Higher doping enhances electrical conductivity due to improved charge carrier pathways.

These findings demonstrate that controlled Ag doping can effectively tailor Fe_2O_3 properties for photocatalytic and optoelectronic applications.

4.Conclusion

In conclusion, the sol-gel synthesis of pure Fe_2O_3 and Ag-doped Fe_2O_3 successfully produced materials with tunable structural, morphological, optical, and electrical properties. XRD confirmed crystalline

phase formation with Ag doping, while SEM revealed morphology changes from spherical to irregular shapes. Surface roughness, particle size distribution, and bonding variations were evident from 3D surface profiles, histograms, and FTIR spectra. UV-Vis analysis showed a redshift and a band gap reduction from 2.3 eV (pure Fe_2O_3) to 2.9 eV (6% Ag-Fe_2O_3). Electrical studies demonstrated enhanced conductivity with increasing Ag content. These improvements highlight the potential of Ag-Fe_2O_3 nanomaterials for advanced applications in electronics, optoelectronics, energy harvesting, batteries, and electrochemical sensors.

5. References

Aithal, P. S., & Aithal, S. (2016). Nanotechnology innovations and commercial applications. *International Journal of Engineering Research and Modern Education (IJERME)*, *1*(1), 751–764.

Ariga, K. (2021). Nanoarchitectonics: What's coming next after nanotechnology? *Nanoscale Horizons*, *6*(6), 364–378. https://doi.org/10.1039/D0NH00655B

Astefanei, A., Núñez, O., & Galceran, M. T. (2015). Characterisation and determination of fullerenes: A critical review. *Analytica Chimica Acta*, *882*, 1–21. https://doi.org/10.1016/j.aca.2015.02.059

Berger, M. (2009). Nanoparticles: Properties, applications and toxicities. *Nanowerk*. Retrieved from https://www.nanowerk.com

Bibi, F., Ali, A., Raza, A., Sultan, M., & Ullah, R. (2020). Structural, optical and magnetic properties of hematite nanoparticles synthesized via sol–gel method. *Materials Research Express*, *7*(1), 015010. https://doi.org/10.1088/2053-1591/ab65e1

Chen, G., Wang, Y., & Wang, L. (2016). A review of nanomaterial synthesis using physical methods. *Nano-Micro Letters*, *8*(1), 1–10. https://doi.org/10.1007/s40820-015-0066-x

Cullity, B. D., & Stock, S. R. (2001). *Elements of X-ray diffraction* (3rd ed.). Prentice Hall.

Drexler, K. E. (1986). *Engines of creation: The coming era of nanotechnology*. Anchor Books.

Dutta, R. K., Basak, S., & Mandal, S. (2018). Effect of silver doping on structural, optical, and catalytic properties of hematite nanoparticles. *Journal of Alloys and Compounds*, *744*, 337–345. https://doi.org/10.1016/j.jallcom.2018.02.159

Ealia, S. A. M., & Saravanakumar, M. P. (2017). A review on the classification, characterisation, synthesis of nanoparticles and their application. *IOP Conference Series: Materials Science and Engineering*, *263*(3), 032019. https://doi.org/10.1088/1757-899X/263/3/032019

Evanoff, D. D., Jr., & Chumanov, G. (2005). Synthesis and optical properties of silver nanoparticles and arrays. *ChemPhysChem*, *6*(7), 1221–1231. https://doi.org/10.1002/cphc.200500113

Goldstein, J., Newbury, D. E., Michael, J. R., Ritchie, N. W. M., Scott, J. H. J., & Joy, D. C. (2018). *Scanning electron microscopy and X-ray microanalysis* (4th ed.). Springer. https://doi.org/10.1007/978-1-4939-6676-9

Ibhadon, A. O., & Fitzpatrick, P. (2013). Heterogeneous photocatalysis: Recent advances and applications. *Catalysts*, *3*(1), 189–218. https://doi.org/10.3390/catal3010189

Ijaz, I., Gilani, E., Nazir, A., & Bukhari, A. (2020). Detail review on chemical, physical and green synthesis, classification, characterizations and applications of nanoparticles. *Green Chemistry Letters and Reviews*, *13*(3), 223–245. https://doi.org/10.1080/17518253.2020.1802517

Khalil, A. T., Ovais, M., Ullah, I., Ali, M., Shinwari, Z. K., & Hassan, D. (2017). Synthesis and characterization of silver-doped Fe_2O_3 nanoparticles and their biomedical applications. *Nanomedicine*, *12*(19), 2361–2374. https://doi.org/10.2217/nnm-2017-0159

Kumar, A., Sharma, R., & Thakur, P. (2020). Influence of silver doping on structural, optical and magnetic properties of Fe_2O_3

nanoparticles. *Journal of Materials Science: Materials in Electronics*, *31*, 13030–13042. https://doi.org/10.1007/s10854-020-03781-1

Nair, M., Gopi, C. V. V. M., & Kim, H. J. (2022). Silver doped metal oxides for photocatalytic and energy applications: A review. *Materials Today: Proceedings*, *60*, 173–180. https://doi.org/10.1016/j.matpr.2021.10.420

Nayak, A. K., Swain, S. K., & Behera, A. (2019). Influence of silver doping on the structural and photocatalytic properties of iron oxide nanoparticles. *Materials Chemistry and Physics*, *223*, 383–391. https://doi.org/10.1016/j.matchemphys.2018.11.070

Ravichandran, K., Valanarasu, S., & Ramya, R. (2019). Enhanced electrical conductivity of Ag-doped metal oxide nanostructures for optoelectronic device applications. *Materials Research Express*, *6*(6), 065901. https://doi.org/10.1088/2053-1591/ab06ad

Sharma, A., Kaushal, A., & Singh, P. (2021). Morphological and structural evolution in metal oxide nanoparticles: Effect of dopants. *Ceramics International*, *47*(3), 3320–3330. https://doi.org/10.1016/j.ceramint.2020.09.269

Sutradhar, P., Debnath, N., & Saha, M. (2014). Sol–gel synthesis of metal oxide nanoparticles: A review. *Journal of Sol-Gel Science and Technology*, *71*, 1–20. https://doi.org/10.1007/s10971-014-3335-1

Taniguchi, N. (1974). On the basic concept of nanotechnology. *Proceedings of the International Conference on Production Engineering*, Japan Society of Precision Engineering, Tokyo, 18–23.

Tauc, J. (1974). *Amorphous and liquid semiconductors*. Springer. https://doi.org/10.1007/978-1-4615-8705-7

Ullah, R., Bibi, F., Ali, A., Sultan, M., & Khan, M. I. (2021). Effect of synthesis method on structural and magnetic properties of α-Fe_2O_3 nanoparticles. *Journal of Materials Science: Materials in Electronics*, *32*, 12734–12744. https://doi.org/10.1007/s10854-021-05727-8

Wang, Z. L., & Xia, Y. N. (2004). Bottom-up and top-down approaches to the synthesis of nanostructures. *Journal of Nanoscience and Nanotechnology*, *4*(4), 254–288. https://doi.org/10.1166/jnn.2004.034

Yuan, W., Li, C., & Lin, S. (2019). Carbon-based nanomaterials for environmental remediation. *Environmental Science: Nano*, *6*(5), 1317–1344. https://doi.org/10.1039/C9EN00047A